Journal of Rock Mechanics and Geotechnical Engineering xxx (xxxx) xxx

Contents lists available at ScienceDirect

Journal of Rock Mechanics and Geotechnical Engineering

journal homepage: www.jrmge.cn

Full Length Article

A particle-resolved heat-particle-fluid coupling model by DEM-IMB-LBM

Ming Xia [a,b], Jinlong Fu [b,*], Y.T. Feng [b], Fengqiang Gong [c], Jin Yu [d]

[a] Hunan Key Laboratory of Geomechanics and Engineering Safety, Xiangtan University, Xiangtan, 411105, China
[b] Zienkiewicz Institute for Modelling, Data and AI, Swansea University, Swansea, SA1 8EP, UK
[c] School of Civil Engineering, Southeast University, Nanjing, 211189, China
[d] Fujian Research Center for Tunneling and Urban Underground Space Engineering, Huaqiao University, Xiamen, 361021, China

ARTICLE INFO

Article history:
Received 26 December 2022
Received in revised form
4 February 2023
Accepted 16 February 2023
Available online xxx

Keywords:
Particle-fluid interaction
Heat transfer
Discrete element method (DEM)
Lattice Boltzmann method (LBM)
Dirichlet-type thermal boundary
Direct numerical simulation

ABSTRACT

Multifield coupling is frequently encountered and also an active area of research in geotechnical engineering. In this work, a particle-resolved direct numerical simulation (PR-DNS) technique is extended to simulate particle-fluid interaction problems involving heat transfer at the grain level. In this extended technique, an immersed moving boundary (IMB) scheme is used to couple the discrete element method (DEM) and lattice Boltzmann method (LBM), while a recently proposed Dirichlet-type thermal boundary condition is also adapted to account for heat transfer between fluid phase and solid particles. The resulting DEM-IBM-LBM model is robust to simulate moving curved boundaries with constant temperature in thermal flows. To facilitate the understanding and implementation of this coupled model for non-isothermal problems, a complete list is given for the conversion of relevant physical variables to lattice units. Then, benchmark tests, including a single-particle sedimentation and a two-particle drafting-kissing-tumbling (DKT) simulation with heat transfer, are carried out to validate the accuracy of our coupled technique. To further investigate the role of heat transfer in particle-laden flows, two multiple-particle problems with heat transfer are performed. Numerical examples demonstrate that the proposed coupling model is a promising high-resolution approach for simulating the heat-particle-fluid coupling at the grain level.

© 2023 Institute of Rock and Soil Mechanics, Chinese Academy of Sciences. Production and hosting by Elsevier B.V. This is an open access article under the CC BY-NC-ND license (http://creativecommons.org/licenses/by-nc-nd/4.0/).

1. Introduction

Particle-fluid interaction problems are commonly encountered in the fields of geosciences, petroleum engineering, geotechnical engineering, and chemical engineering, to name but a few. Due to the complex and intricate nature of a particle-fluid problem, it is very difficult, if not impossible, to obtain its analytical solutions. Alternatively, numerical methods are always used to obtain approximate solutions for such problems. Since there are a large number of moving particles involved, it is natural to use the discrete element method (DEM) to describe particle-particle interactions. On the other hand, the computational fluid dynamics (CFD) and the lattice Boltzmann method (LBM), which can be used to simulate fluid flows, have been coupled with DEM to study such coupled and highly nonlinear problems.

Currently, the unresolved DEM-CFD, where the empirical hydrodynamic forces are based on averaging techniques, is commonly used for large-scale engineering simulations due to its relatively high computational efficiency (Wang et al., 2022b). In contrast, the high-resolution DEM-LBM and the fully-resolved DEM-CFD with fine fluid grids are mainly used to investigate the physical/mechanical mechanism from a mesoscopic/microscopic point of view (Feng and Michaelides, 2008; Han and Cundall, 2013). Due to the high efficiency of high-resolution DEM-LBM compared to fully-resolved DEM-CFD, the former has attracted more and more attention in the geomechanics research community over the past two decades (Cook et al., 2004; Feng et al., 2007, 2010; Owen et al., 2011; Galindo-Torres, 2013; Han and Cundall, 2013; Zhang et al., 2016, 2017; Wang et al., 2017a, 2019, 2020, 2021, 2022a, 2023; Honari and Seyedi Hosseininia, 2021).

To ensure a non-slip condition at moving particle surfaces, various coupling schemes, such as the modified bounce-back (MBB) (Ladd, 1994), interpolated bounce-back (IBB) (Chun and Ladd, 2007), immersed boundary method (IBM) (Peskin, 1977) and immersed moving boundary (IMB) method (Noble and Torczynski,

* Corresponding author.
E-mail address: jinlong.fu@swansea.ac.uk (J. Fu).
Peer review under responsibility of Institute of Rock and Soil Mechanics, Chinese Academy of Sciences.

https://doi.org/10.1016/j.jrmge.2023.02.030
1674-7755 © 2023 Institute of Rock and Soil Mechanics, Chinese Academy of Sciences. Production and hosting by Elsevier B.V. This is an open access article under the CC BY-NC-ND license (http://creativecommons.org/licenses/by-nc-nd/4.0/).

Please cite this article as: Xia M et al., A particle-resolved heat-particle-fluid coupling model by DEM-IMB-LBM, Journal of Rock Mechanics and Geotechnical Engineering, https://doi.org/10.1016/j.jrmge.2023.02.030

1998) have been used to couple DEM and LBM. As a natural next step, these coupling schemes have been extended from isothermal problems to non-isothermal problems to ensure a Dirichlet-type, Neumann-type or Robin-type condition on moving particle surfaces. Hu and Guo (2017) proposed a multi-step iterative IBB with Dirichlet-type thermal boundary condition to update the distribution functions for temperature at fluid nodes and boundary nodes with links to other fluid nodes. Rosemann et al. (2019) developed a new IBB to treat Dirichlet-type thermal boundary condition for the heat transfer between particles and fluid. Liu and Wu (2019) adopted the MBB for Dirichlet thermal boundary condition to simulate the inertial migration of a neutrally buoyant circular particle in a planar Poiseuille flow with thermal convection.

However, the MBB and IBB are non-local, as the information from neighboring nodes is required. On the contrary, the IBM and IMB are local operators. Kang and Hassan (2011) proposed a direct-forcing IBM with Dirichlet-type thermal boundary for thermal LBM to simulate non-isothermal flows. Hu et al. (2016) proposed a diffuse-interface IBM to simulate three different thermal boundary conditions in thermal flow problems. Tao et al. (2021) proposed a distribution function correction-based IBM with Dirichlet-type thermal boundary for thermal particle flows, in which the boundary condition is directly implemented by correcting the distribution function at the neighboring points around the interface. Furthermore, an adjustment parameter is introduced to ensure the accuracy in the boundary treatment. Zhang et al. (2015) proposed a coupled DEM-IBM-LBM model for simulating heat transfer in a particle-fluid system. However, only the Dirichlet thermal boundary condition is considered in this model. Suzuki et al. (2018) constructed a two-dimensional thermal IBM-LBM for moving-boundary flows with heat transfer. Both the Dirichlet and Neumann conditions can be considered. McCullough et al. (2020) simulated particle suspensions using the DEM-IMB-LBM model. In this model, the temperature-dependent fluid viscosity is accounted for. However, heat transfer between particles and fluid is not considered. Recently, McCullough et al. (2021) implemented an appropriate conjugate-type thermal boundary condition to ensure conjugate heat transfer at the interface of fluid and moving particles. In this approach, continuity of both temperature and heat flux is maintained at the interface. However, the interface boundary condition used by McCullough et al. (2021) is non-local, which not only requires neighboring node information at each step, but also requires identifying the exact direction between the current node and its nearest neighbor with the adjacent media. Therefore, this boundary condition cannot be used to modeling Dirichlet-type thermal flow problems directly.

To the best knowledge of the authors, a coupled DEM-IMB-LBM model for numerically simulating particle-fluid interaction problems with heat transfer between fluid and particles is still lacking. Recently, Chen and Müller (2020) proposed a Dirichlet-type thermal boundary condition, which can accurately capture heat convection for curved moving boundaries between particles and fluid. The aim of this work is to develop *a thermal DEM-IMB-LBM model* based on the *adaptation of the Dirichlet-type thermal boundary condition* for the simulation of particle-laden flows involving *heat transfer*. The major difference between the work of Chen and Müller (2020) and the present work is that: the model in Chen and Müller (2020) is in the thermal LBM framework, while the present work is in the DEM-LBM framework. Thus, the present work can not only modeling multi-particles contact and motion, but also consider heat transfer during particle motion. In addition, Xia et al. (2023) have proposed a DEM-IMB-LBM approach to modeling methane hydrate exploitation associated with mass transport and particle dissolution. However, the present study focuses on heat transfer with consideration of temperature-dependent fluid density, which is completely different from Xia et al. (2023).

The rest of the paper is organized as follows. In Section 2, a detailed introduction of the coupled thermal LBM and DEM, including both force interactions and heat transfer between solid particles and the fluid phase, will be given. In Section 3, two benchmark tests, a single-particle sedimentation with heat transfer and a two-particle drafting-kissing-tumbling (DKT) simulation with heat transfer, are performed to validate the proposed technique. In Section 4, the role of heat transfer in particle-laden flows is further investigated by applying the proposed model to simulate complicated particle-fluid interaction problems with multiple particles. Finally, the main contributions of this study are summarized in Section 5.

2. Methodologies

In this section, a coupled thermal lattice Boltzmann-discrete element model by IMB is developed based on adapting the Dirichlet-type thermal boundary condition for the numerical simulations of particle-laden flows with heat transfer, as graphically illustrated in Fig. 1. Detailed explanations about this particle-resolved coupling method, with focus on the IMB for heat transfer between solid particles and the fluid phase, are provided below.

2.1. Discrete element method (DEM)

The DEM was proposed to simulate the geomaterial at the grain level by Cundall and Strack (1979). The macroscopic mechanical behavior of the geomaterials can be reproduced by solving the contact forces applied to individual particles and their subsequent movement (Qu et al., 2022). Newton's second law is used to update

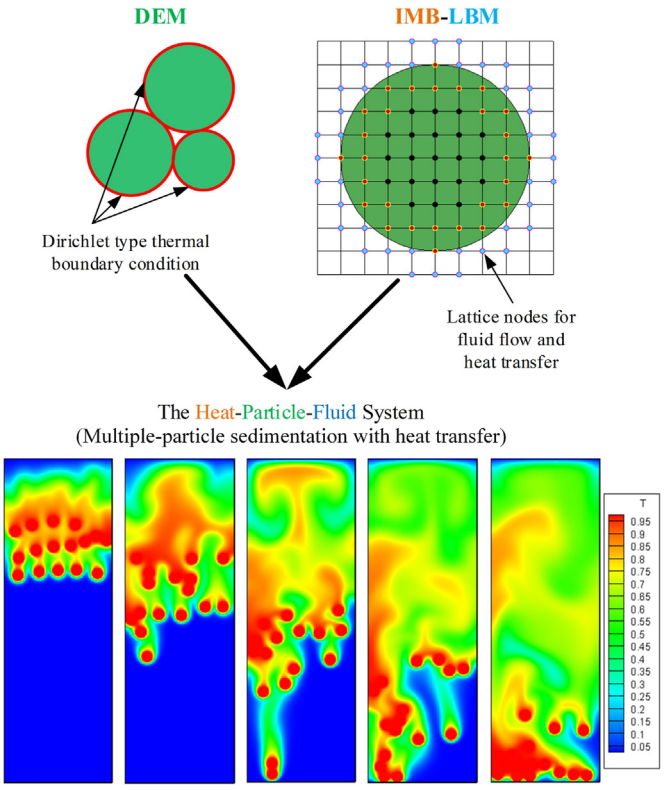

Fig. 1. Graphical illustration of the developed DEM-IMB-LBM model coupled with heat transfer (unit: the lattice unit).

Please cite this article as: Xia M et al., A particle-resolved heat-particle-fluid coupling model by DEM-IMB-LBM, Journal of Rock Mechanics and Geotechnical Engineering, https://doi.org/10.1016/j.jrmge.2023.02.030

the particle movement, while the contact force is calculated by the linear contact law based on contact mechanics. The DEM and related computational algorithms have been described in detail in the literature (O'Sullivan, 2011; Feng, 2021a, b, 2023). For the sake of completeness, only a brief summary of some of the key equations will be presented here.

The movement, including translation and rotation, of a particle is described by the following equations:

$$m\ddot{\boldsymbol{u}}_{\mathrm{p}} = \boldsymbol{F}_{\mathrm{c}} + \boldsymbol{F}_{\mathrm{G}} + \boldsymbol{F}_{\mathrm{f}} \tag{1}$$

$$I\ddot{\boldsymbol{\theta}} = \boldsymbol{T}_{\mathrm{c}} + \boldsymbol{T}_{\mathrm{f}} \tag{2}$$

where m and I are the mass and the moment of inertia of the particle, respectively; $\boldsymbol{u}_{\mathrm{p}}$ and $\boldsymbol{\theta}$ are the particle displacement and rotation angle, respectively; $\boldsymbol{F}_{\mathrm{c}}$ and $\boldsymbol{T}_{\mathrm{c}}$ are the resultant contact force and resultant torque from other particles and/or boundary walls, respectively; $\boldsymbol{F}_{\mathrm{G}}$ is the gravitational force; $\boldsymbol{F}_{\mathrm{f}}$ and $\boldsymbol{T}_{\mathrm{f}}$ are the hydrodynamics force and torque, respectively, which will be given in Section 2.3.

The contact force $\boldsymbol{F}_{\mathrm{c}}$ can be decomposed into normal and tangential components, $\boldsymbol{F}_{\mathrm{c}}^{\mathrm{n}}$ and $\boldsymbol{F}_{\mathrm{c}}^{\mathrm{t}}$, and are calculated as follows:

$$\boldsymbol{F}_{\mathrm{c}} = \boldsymbol{F}_{\mathrm{c}}^{\mathrm{n}} + \boldsymbol{F}_{\mathrm{c}}^{\mathrm{t}} = F_{\mathrm{c}}^{\mathrm{n}}\boldsymbol{n} + F_{\mathrm{c}}^{\mathrm{t}}\boldsymbol{t} \tag{3}$$

$$F_{\mathrm{c}}^{\mathrm{n}} = k_{\mathrm{n}}u_{\mathrm{n}} \tag{4}$$

$$F_{\mathrm{c}}^{\mathrm{t}} = \left(F_{\mathrm{c}}^{\mathrm{t}}\right)_{\mathrm{previous}} - k_{\mathrm{t}}\Delta u_{\mathrm{t}} \tag{5}$$

$$\left|F_{\mathrm{c}}^{\mathrm{t}}\right| \le \mu\left|F_{\mathrm{c}}^{\mathrm{n}}\right| \tag{6}$$

where $\boldsymbol{n}$ and $\boldsymbol{t}$ are the unit normal and tangential vectors, respectively; k_{n} and k_{t} are the normal and tangential contact stiffnesses, respectively; u_{n} and Δu_{t} are the normal contact displacement and incremental tangential contact displacement at current time step, respectively; and μ is the coefficient of friction.

2.2. Lattice Boltzmann method (LBM) for fluid flow and heat transfer

The LBM is a mesoscopic method for modeling fluid flows (Qian et al., 1992), in which the fluid phase is treated as an assembly of fluid particle clusters resided at the node of lattice grids. There are two primary processes for the imaginary (fluid) particles. A collision process is used to solve the interaction of fluid particles, while a streaming process is utilized to achieve fluid flow (Fu et al., 2020).

When the coupling between the fluid flow and heat transfer is considered in particle-fluid interaction problems, the Boussinesq approximation is adopted, in which the fluid density is assumed to be a linear function of temperature:

$$\rho_{\mathrm{f}} = \rho_{\mathrm{f0}}[1 - \beta_T(T - T_0)] \tag{7}$$

where ρ_{f} is the fluid density, ρ_{f0} is the reference fluid density, T is the fluid temperature, T_0 is the reference fluid temperature, and β_T is the thermal expansion coefficient of fluid.

When the Boussinesq approximation is considered, the buoyancy force induced by temperature-dependent density of fluid should be implemented appropriately. Thus, the corresponding density and temperature distribution functions, f_i and g_i, can be solved by using a single-relaxation-time BGK model as follows:

$$f_i(\boldsymbol{x} + \boldsymbol{e}_i\Delta t, t + \Delta t) = f_i(\boldsymbol{x}, t) + \Omega_i^{\mathrm{f}} + \Delta t F_i \ (i = 0, 1, \ldots, 8) \tag{8}$$

$$g_i(\boldsymbol{x} + \boldsymbol{e}_i\Delta t, t + \Delta t) = g_i(\boldsymbol{x}, t) + \Psi_i^{\mathrm{f}} \ (i = 0, 1, \ldots, 4) \tag{9}$$

$$\Omega_i^{\mathrm{f}} = -\frac{\Delta t}{\tau_{\mathrm{f}}}\left[f_i(\boldsymbol{x}, t) - f_i^{\mathrm{eq}}(\boldsymbol{x}, t)\right] \tag{10}$$

$$\Psi_i^{\mathrm{f}} = -\frac{\Delta t}{\tau_{\mathrm{g}}}\left[g_i(\boldsymbol{x}, t) - g_i^{\mathrm{eq}}(\boldsymbol{x}, t)\right] \tag{11}$$

$$F_i = \left(1 - \frac{\Delta t}{2\tau_{\mathrm{f}}}\right)\omega_{\mathrm{f}i}\left[\frac{\boldsymbol{e}_i - \boldsymbol{u}}{c_{\mathrm{s}}^2} + \frac{(\boldsymbol{e}_i \cdot \boldsymbol{u})\boldsymbol{e}_i}{c_{\mathrm{s}}^4}\right] \cdot \boldsymbol{F} \tag{12}$$

$$\boldsymbol{F} = -\rho_{\mathrm{f0}}\beta_T(T - T_0)\boldsymbol{g} \tag{13}$$

where for any grid node $\boldsymbol{x}$, $\boldsymbol{x} + \boldsymbol{e}_i\Delta t$ is its nearest neighboring node along direction i with discrete velocity $\boldsymbol{e}_i$; f_i^{eq} is the equilibrium density distribution function; g_i^{eq} is the equilibrium temperature distribution function; Ω_i^{f} and Ψ_i^{f} are the collision operators for density and temperature, respectively; τ_{f} and τ_{g} are the dimensionless relaxation times of density and temperature, respectively; F_i is the buoyancy force term; Δt is the time step of LBM; $\boldsymbol{g} = (g_x, g_y)$ is the gravity acceleration vector; $\boldsymbol{F}$ is the buoyancy force density; and $\omega_{\mathrm{f}i}$ is the weighting factor with $\omega_{\mathrm{f0}} = 4/9$, $\omega_{\mathrm{f1-f4}} = 1/9$, and $\omega_{\mathrm{f5-f8}} = 1/36$.

According to Eq. (7), the buoyancy force in Eq. (12) is implemented similar to the body force proposed by Guo et al. (2002), which indicates the effect of temperature on fluid flow behavior through Eq. (8).

In this work, the commonly used D2Q9 model is adopted for the fluid flow as shown in Fig. 2a, and a D2Q5 model is employed to simulate heat transfer as shown in Fig. 2b. Compared with the D2Q9 model, the D2Q5 model could reduce the computational cost and keep an acceptable accuracy for modeling advection-diffusion problems (Kang et al., 2007). The fluid particles at each node are only allowed to move to its immediate neighboring nodes or stay at rest with velocities $\boldsymbol{e}_i$ (i = 0, 1, …, 8), as graphically illustrated in Fig. 2. The velocities of fluid particles are defined as follows:

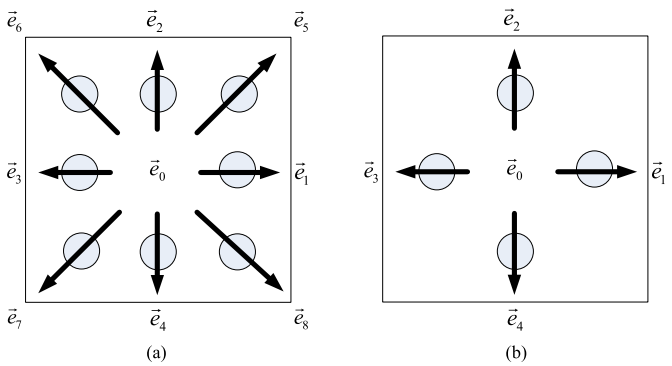

Fig. 2. LBM for fluid flow with D2Q9 model (a) and heat transfer with D2Q5 model (b).

Please cite this article as: Xia M et al., A particle-resolved heat-particle-fluid coupling model by DEM-IMB-LBM, Journal of Rock Mechanics and Geotechnical Engineering, https://doi.org/10.1016/j.jrmge.2023.02.030

$$\boldsymbol{e}_i = \begin{cases} (0,0) & (i = 0) \\ c\left(\cos\dfrac{(i-1)\pi}{2}, \sin\dfrac{(i-1)\pi}{2}\right) & (i = 1,2,3,4) \\ \sqrt{2}c\left(\cos\dfrac{(2i-9)\pi}{4}, \sin\dfrac{(2i-9)\pi}{4}\right) & (i = 5,6,7,8) \end{cases} \tag{14}$$

The equilibrium density- and temperature-distribution functions (f_i^{eq} and g_i^{eq}) are calculated as

$$f_i^{\mathrm{eq}} = \omega_{\mathrm{fi}}\rho_{\mathrm{f}}\left[1 + \frac{3}{c^2}\boldsymbol{e}_i \cdot \boldsymbol{u} + \frac{9}{2c^4}(\boldsymbol{e}_i \cdot \boldsymbol{u})^2 - \frac{3}{2c^2}\boldsymbol{u} \cdot \boldsymbol{u}\right] \ (i = 0, 1, \ldots, 8) \tag{15}$$

$$g_i^{\mathrm{eq}} = \omega_{\mathrm{g}i}T\left[1 + \frac{3}{c^2}\boldsymbol{e}_i \cdot \boldsymbol{u}\right] \ (i = 0, 1, \ldots, 4) \tag{16}$$

where $\boldsymbol{u} = (u_x, u_y)$ is the velocity vector; ω_{gi} is the weighting factor with $\omega_{\mathrm{g}0} = 1/3$ and $\omega_{\mathrm{g}1-\mathrm{g}4} = 1/6$; and $c\,(= h/\Delta t)$ is the lattice speed with h and Δt being the lattice spacing and time step, respectively.

The macroscopic fluid variables, i.e. density, velocity and temperature, can be recovered from the distribution functions by

$$\rho_{\mathrm{f}} = \sum_{i=0}^{8} f_i \tag{17}$$

$$\rho_{\mathrm{f}}\boldsymbol{u} = \sum_{i=0}^{8} f_i\boldsymbol{e}_i + \frac{\Delta t}{2}\boldsymbol{F} \tag{18}$$

$$T = \sum_{i=0}^{4} g_i \tag{19}$$

The fluid pressure field is determined by the following equation of state $p = c_{\mathrm{s}}^2\rho_{\mathrm{f}}$, where c_{s} is termed the fluid speed of sound and is related to the lattice speed $c = h/\Delta t$ by $c_{\mathrm{s}} = c/\sqrt{3}$ in the D2Q9 model.

The kinematic viscosity and thermal diffusion coefficient are calculated by

$$\nu = \frac{1}{3}\left(\tau_{\mathrm{f}} - 0.5\right)\frac{h^2}{\Delta t} \tag{20}$$

$$\alpha = \frac{1}{3}\left(\tau_{\mathrm{g}} - 0.5\right)\frac{h^2}{\Delta t} \tag{21}$$

where ν is the kinematic viscosity coefficient, and α is the thermal diffusion coefficient. Note that in the present study, the kinematic viscosity of fluid is a constant in Eq. (20). However, a temperature-dependent viscosity of fluid can be considered (McCullough et al., 2020). A detailed study on the viscosity-dependence and convergence of the present model will be an ideal path for future study (Chun and Ladd, 2007; Wang et al., 2018).

2.3. Fluid-particle interaction and heat transfer

The IMB scheme for DEM-LBM coupling was proposed by Noble and Torczynski (1998) by a smooth representation of solid particle boundaries. In this scheme, the lattice Boltzmann equation for the fluid flow (i.e. Eq. (8)) is modified by incorporating a collision operator Ω_i^{s} for fluid nodes partially covered by the solid, and its specific form including the buoyancy term can be given by

$$f_i(\boldsymbol{x} + \boldsymbol{e}_i\Delta t, t + \Delta t) = f_i(\boldsymbol{x}, t) + \left(1 - B_{\mathrm{f}}\right)\Omega_i^{\mathrm{f}} + B_{\mathrm{f}}\Omega_i^{\mathrm{s}} + \left(1 - B_{\mathrm{f}}\right)\Delta t F_i \tag{22}$$

$$B_{\mathrm{f}} = \frac{\gamma\left(\tau_{\mathrm{f}} - 0.5\right)}{(1-\gamma) + \left(\tau_{\mathrm{f}} - 0.5\right)} \tag{23}$$

$$\Omega_i^{\mathrm{s}} = f_{-i}(\boldsymbol{x}, t) - f_i(\boldsymbol{x}, t) + f_i^{\mathrm{eq}}\left(\rho_{\mathrm{f}}, \boldsymbol{u}_{\mathrm{b}}\right) - f_{-i}^{\mathrm{eq}}\left(\rho_{\mathrm{f}}, \boldsymbol{u}\right) \tag{24}$$

where B_{f} is a weighting function and depends on the relaxation time of the density τ_{f} ($B_{\mathrm{f}} = 0$ and 1 corresponding to a pure fluid node and a pure solid node, respectively) and the local nodal solid ratio γ, Ω_i^{s} is the collision operator associated with the fluid flow in the i-th direction for nodes partially covered by solid, $-i$ denotes the opposite direction of i, and $\boldsymbol{u}_{\mathrm{b}}$ is the velocity of the corresponding particle at the node.

The total hydrodynamic force and torque exerted on a particle are summed up as

$$\boldsymbol{F}_{\mathrm{f}} = ch\left[\sum_n\left(B_{\mathrm{f}}^n\sum_i\Omega_i^{\mathrm{s}}\boldsymbol{e}_i\right)\right] \tag{25}$$

$$\boldsymbol{T}_{\mathrm{f}} = ch\left[\sum_n(\boldsymbol{x}_n - \boldsymbol{x}_{\mathrm{c}}) \times \left(B_f^{\mathrm{n}}\sum_i\Omega_i^{\mathrm{s}}\boldsymbol{e}_i\right)\right] \tag{26}$$

where $\boldsymbol{x}_n$ and $\boldsymbol{x}_{\mathrm{c}}$ are the coordinates of the boundary node n and particle center, respectively.

Recently, the thermal Dirichlet-type boundary was solved using an IMB by Chen and Müller (2020). This new thermal boundary condition has three prominent advantages: the pure locality of the collision operator, the simple linear streaming operator, and second order accuracy. Therefore, it is promising for simulating heat transfer in particle-fluid systems involving large number of moving curved boundaries. For this thermal boundary condition, the lattice Boltzmann equation for heat transfer between the fluid and solid particles (i.e. Eq. (9)) is modified to include a collision operator for nodes covered by the fluid and solid particles at the same time, Ψ_i^{s}, and can be written as

$$g_i(\boldsymbol{x} + \boldsymbol{e}_i\Delta t, t + \Delta t) = g_i(\boldsymbol{x}, t) + (1 - B_{\mathrm{g}})\Psi_i^{\mathrm{f}} + B_{\mathrm{g}}\Psi_i^{\mathrm{s}} \tag{27}$$

$$B_{\mathrm{g}} = \frac{\gamma(\tau_{\mathrm{g}} - 0.5)}{(1-\gamma) + (\tau_{\mathrm{g}} - 0.5)} \tag{28}$$

$$\Psi_i^{\mathrm{s}} = -g_{-i}(\boldsymbol{x}, t) - g_i(\boldsymbol{x}, t) + g_i^{\mathrm{eq}}(T_{\mathrm{b}}, \boldsymbol{u}) + g_{-i}^{\mathrm{eq}}(T, \boldsymbol{u}) \tag{29}$$

where B_{g} is a weighting function and depends on the local solid ratio γ and relaxation time τ_{g} of the temperature ($B_{\mathrm{g}} = 0$ and 1 corresponding to a pure fluid node and a pure solid node, respectively), Ψ_i^{s} is the collision operator for solid nodes associated with heat transfer in the i direction, and T_{b} is the corresponding particle temperature at the node.

2.4. Coupling procedures and unit conversions

When coupling DEM with LBM, a sub-cycling algorithm is often used (Feng et al., 2007), because the timestep of DEM is normally smaller than that of LBM. The coupling procedure of thermal DEM-

Please cite this article as: Xia M et al., A particle-resolved heat-particle-fluid coupling model by DEM-IMB-LBM, Journal of Rock Mechanics and Geotechnical Engineering, https://doi.org/10.1016/j.jrmge.2023.02.030

IMB-LBM is given in Table 1. As DEM is coupled with LBM through IMB scheme, four types of nodes (solid boundary, interior solid, fluid boundary, and fluid) should be identified at each LBM step. To further improve the computational efficiency, a robust and more efficient searching algorithm proposed by Wang et al. (2019) can be used in the whole computation.

In our code, to improve the computational efficiency, the lattice units are used for all physical quantities. The conversion, for isothermal problems, between physical units and lattice units can be found in Feng et al. (2007). For non-isothermal problems, the relationship is given for the conversion of the variables used in the coupled thermal DEM-IMB-LBM model in Table 2 (Xia, 2016), where superscripts '*p*' and '*LB*' are used to indicate a variable in the physical units and lattice units, respectively.

3. Numerical model validation

For the verification purpose, the coupled thermal DEM-IMB-LBM model described in the above section is applied to two examples: single-particle and two-particle sedimentation with heat transfer in an enclosure. The following dimensionless numbers and parameters are defined:

$$Re = \frac{U_{\mathrm{ref}} L_{\mathrm{ref}}}{\nu}, Pr = \frac{\nu}{\alpha}, Gr = \frac{\left|g_{\mathrm{y}}\right| \beta_T L_{\mathrm{ref}}^3 (T_{\mathrm{b}} - T_0)}{\nu^2}, \rho_{\mathrm{r}} = \frac{\rho_{\mathrm{s}}}{\rho_{\mathrm{f0}}} \tag{30}$$

where Re is the Reynolds number, Pr is the Prandtl number, Gr is the Grashof number, ρ_{r} is the ratio of the particle density to the fluid density, ρ_{s} is the particle density, T_{b} is the particle temperature, L_{ref} is the reference scale equal to the diameter of a particle ($= 2R_{\mathrm{p}}$), and U_{ref} is the reference velocity.

3.1. Single-particle sedimentation with heat transfer

The first benchmark test is the sedimentation of a hot/cold particle with constant temperature, adopted from Feng and Michaelides (2008). As shown in Fig. 3, the computational domain is 0.16 m in width and 0.4 m in height, and is divided into 160 × 400 lattice grids with spacing $h = 0.001$ m. The four boundaries are static walls and thus the no-slip boundary condition is imposed, and are also fully insulated. A particle initially located at the position (0.08 m, 0.36 m) moves downward due to gravity. For the fluid, the kinematic viscosity is 1×10^{-5} m^2/s, the density is 1000 kg/m^3, the thermal diffusivity is 1×10^{-5} m^2/s, and the thermal expansion coefficient is 1.02×10^{-4} K^{-1}. The particle radius is 0.005 m. The density of the particle varies in the range of 1001–1100 kg/m^3, resulting in the density ratio (ρ_{r}) in the range of 1.001–1.1. According to Eq. (30), the corresponding Re number is in the range of 12.4–124.

The time step for LBM and DEM are respectively 0.1×10^{-2} s and 0.8197×10^{-5} s, resulting in a sub-cycling number of DEM (N_{sub}) in an LBM time step to be 122. Both relaxation time for density (τ_{f}) and temperature (τ_{g}) are 0.53, indicating that the Prandtl number Pr is 1. The initial temperature of fluid (T_0) is 290 K, while three different initial temperatures of the particle ($T_{\mathrm{b}} = 280$, 290 and 300 K) are considered. The particle temperature is uniform and constant during the whole simulation process. Correspondingly, according to Eq. (30), three situations with different Grashof numbers Gr are investigated: $Gr = -100$ (a colder particle), $Gr = 0$ (an isothermal particle) and $Gr = 100$ (a hotter particle).

To compare our numerical results with those of Feng and Michaelides (2008), the following three parameters are calculated as follows:

$$Re_{\mathrm{t}} = \frac{U_{\mathrm{t}} L_{\mathrm{ref}}}{\nu}, C_{\mathrm{d}} = \frac{2F_{\mathrm{d}}}{\rho_{\mathrm{f0}} U_{\mathrm{t}}^2 L_{\mathrm{ref}}}, U^* = \frac{U_{\mathrm{t}}}{U_{\mathrm{ref}}}, U_{\mathrm{ref}} = \sqrt{\pi R_{\mathrm{p}} (\rho_{\mathrm{r}} - 1) \left|g_{\mathrm{y}}\right|} \tag{31}$$

Table 1
The coupling procedure of the thermal DEM-IMB-LBM model.

1. Map these particles onto corresponding target cells (forming particle list in each cell)
2. Initialize the fluid field and the temperature field, and identify four sorts of nodes (i.e. solid boundary, interior solid, fluid boundary, and fluid)
3. Loop over LBM iterations
   - 3.1. Loop over DEM sub-cycling
     - 3.1.1. Determine solid particles in each searching cell
     - 3.1.2. Identify the corresponding target cell for solid particles
       - (a) Contact detection for a particle with potential particles in the target cell
       - (b) Calculate contact forces and torques
     - 3.1.3. calculate particle velocity and angular velocity
     - 3.1.4. Update particle movement
   - 3.2. Update four sorts of nodes, and calculate the local solid ratio for each node
   - 3.3. Perform collision process with both the fluid field and the temperature field
     - (a) Fluid nodes using Eqs. (8) and (9)
     - (b) Other three sort nodes using Eqs. (22) and (27)
     - (c) Hydrodynamic forces and torques using Eqs. (25) and (26)
   - 3.4. Apply the bounce-back rule to the lattice nodes occupied by stationary walls and particles
   - 3.5. Perform streaming process for both the fluid field and the temperature field
   - 3.6. Enforce the fluid and temperature boundary conditions

Table 2
The conversions between the physical units and the lattice units associated with the coupled thermal DEM-IMB-LBM model.

Variable name	Physical unit	Lattice unit	Relationship
Fluid density	$\rho_{\mathrm{f}}^{\mathrm{p}}$	$\rho_{\mathrm{f}}^{\mathrm{LB}}$	$\rho_{\mathrm{f}}^{\mathrm{p}} = \rho_{\mathrm{f0}} \rho_{\mathrm{f}}^{\mathrm{LB}}$
Spacing	$h^{\mathrm{p}} = h$	$h^{\mathrm{LB}} = 1$	
Time step for LBM	$\Delta t^{\mathrm{p}} = \Delta t$	$\Delta t^{\mathrm{LB}} = 1$	
Lattice speed	$c^{\mathrm{p}} = h/\Delta t$	$c^{\mathrm{LB}} = 1$	
Coordinate/displacement	$\boldsymbol{x}^{\mathrm{p}}$	$\boldsymbol{x}^{\mathrm{LB}}$	$\boldsymbol{x}^{\mathrm{p}} = h\boldsymbol{x}^{\mathrm{LB}}$
Velocity	$\boldsymbol{u}^{\mathrm{p}}$	$\boldsymbol{u}^{\mathrm{LB}}$	$\boldsymbol{u}^{\mathrm{p}} = \frac{h}{\Delta t}\boldsymbol{u}^{\mathrm{LB}}$
Gravity acceleration	$\boldsymbol{g}^{\mathrm{p}}$	$\boldsymbol{g}^{\mathrm{LB}}$	$\boldsymbol{g}^{\mathrm{p}} = \frac{h}{(\Delta t)^2}\boldsymbol{g}^{\mathrm{LB}}$
Kinematic viscosity	$\boldsymbol{\nu}^{\mathrm{p}}$	$\boldsymbol{\nu}^{\mathrm{LB}}$	$\boldsymbol{\nu}^{\mathrm{p}} = \frac{h^2}{\Delta t}\boldsymbol{\nu}^{\mathrm{LB}}$
Density-distribution function	f_i^{p}	f_i^{LB}	
Temperature-distribution function	g_i^{p}	g_i^{LB}	
Temperature	T^{p}	T^{LB}	$T^{\mathrm{p}} = (T_{\mathrm{max}}^{\mathrm{p}} - T_{\mathrm{min}}^{\mathrm{p}}) T^{\mathrm{LB}} + T_{\mathrm{min}}^{\mathrm{p}}$
Thermal expansion coefficient of fluid	β_T^{p}	β_T^{LB}	$\beta_T^{\mathrm{p}} = \frac{1}{T_{\mathrm{max}}^{\mathrm{p}} - T_{\mathrm{min}}^{\mathrm{p}}} \beta_T^{\mathrm{LB}}$
Thermal diffusion coefficient of fluid	α^{p}	α^{LB}	$\alpha^{\mathrm{p}} = \frac{h^2}{\Delta t}\alpha^{\mathrm{LB}}$
Hydrodynamic force	$\boldsymbol{F}_{\mathrm{f}}^{\mathrm{p}}$	$\boldsymbol{F}_{\mathrm{f}}^{\mathrm{LB}}$	$\boldsymbol{F}_{\mathrm{f}}^{\mathrm{p}} = \frac{h^3}{(\Delta t)^2}\rho_{\mathrm{f0}}\boldsymbol{F}_{\mathrm{f}}^{\mathrm{LB}}$
Hydrodynamic torque	$T_{\mathrm{f}}^{\mathrm{p}}$	$T_{\mathrm{f}}^{\mathrm{LB}}$	$T_{\mathrm{f}}^{\mathrm{p}} = \frac{h^4}{(\Delta t)^2} T_{\mathrm{f}}^{\mathrm{LB}}$
Stiffness	k_n^{p}	k_n^{LB}	$k_n^{\mathrm{p}} = \left(\frac{h}{\Delta t}\right)^2 k_n^{\mathrm{LB}}$
Mass	m^{p}	m^{LB}	$m^{\mathrm{p}} = \rho_{\mathrm{s}}^{\mathrm{p}} h^2 m^{\mathrm{LB}}$
Damping coefficient	$c_{\mathrm{d}}^{\mathrm{p}}$	$c_{\mathrm{d}}^{\mathrm{LB}}$	$c_{\mathrm{d}}^{\mathrm{p}} = \frac{h^2}{\Delta t} c_{\mathrm{d}}^{\mathrm{LB}}$
Critical time step for DEM	$\Delta t_{\mathrm{cr}}^{\mathrm{p}}$	$\Delta t_{\mathrm{cr}}^{\mathrm{LB}}$	$\Delta t_{\mathrm{cr}}^{\mathrm{p}} = \Delta t \Delta t_{\mathrm{cr}}^{\mathrm{LB}}$

Please cite this article as: Xia M et al., A particle-resolved heat-particle-fluid coupling model by DEM-IMB-LBM, Journal of Rock Mechanics and Geotechnical Engineering, https://doi.org/10.1016/j.jrmge.2023.02.030

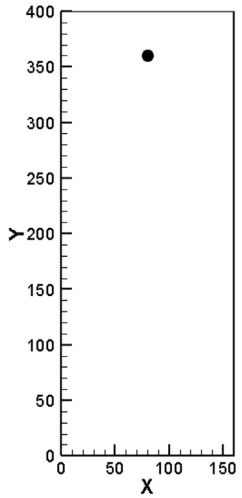

Fig. 3. Single particle sedimentation in an enclosure (unit: the lattice unit).

where Re_t is the Reynolds number based on the terminal velocity (U_t) of the particle, C_d is the drag coefficient, F_d is the steady drag force acting on the particle when it reaches the terminal and steady velocity, and U^* is the dimensionless terminal velocity.

Fig. 4 compares the drag coefficients, the dimensionless terminal velocity and the Mach number (Ma) with the Re number and the Gr number. Fig. 4a shows that with the increase of Re_t, the drag coefficient decreases remarkably when Gr is 0 or 100, while the drag coefficient first increases and then decreases when Gr is -100. From Fig. 4b, we find that with the increase of Re, the dimensionless terminal velocity first decreases and then increases when Gr is -100, while it increases gradually when Gr is 0 or 100. Generally speaking, our numerical results agree well with the experimental results of Tritton (1959) and the numerical results of Feng and Michaelides (2008) and Dan and Wachs (2010).

From Fig. 4b, the dimensionless terminal velocity (U^*) of the particle is 0.0851 when $\rho_r = 1.1$ and $Gr = -100$. In this situation, the velocity of the particle during sedimentation is maximum, and its value (U_{max}) is 0.106 m/s. In this extreme case, the accumulated displacement of the particle (l_{max}) during N_{sub} DEM subcycling can be calculated as follows:

$$l_{max} = U_{max} N_{sub} \Delta t_{DEM} = 0.106 \times 122 \times 0.8197 \times 10^{-5} = 0.106 \times 10^{-3}\ \text{m} \quad (32)$$

As stated by Owen et al. (2011) and Honari and Seyedi Hosseininia (2021), a practical limit on the subcycling number is required to ensure the accuracy of the DEM-IMB-LBM model. From Eq. (32), since the accumulated displacement of particle (l_{max}) is much lower than a one grid cell h (i.e. 0.001 m), the present high value for the sub-cycling number ($N_{sub} = 122$) is still accurate for modeling the present problem.

One important source of error in LBM simulations is the compressibility of fluid, which is often controlled by monitoring the Mach number (Ma) and/or the density changes of fluid throughout the simulation. It is often required $Ma \ll 1$. In practice, Ma should be, at least, smaller than 0.1 (Chen and Doolen, 1998; Feng et al., 2007). As shown in Fig. 4c, all Ma numbers are small than 0.1, indicating that the results obtained are reasonably accurate.

On the other hand, Ma increases as Gr decreases, indicating that Ma is affected by Gr number. However, the amount of change is small, which means that the density fluctuation due to temperature change does not lead to high compressibility errors in the models. The reason for this is that, according to Eq. (7), the maximum fluid density change of the initial density can be calculated as $|\Delta\rho_f/\rho_{f0}| = |\rho_f - \rho_{f0}|/\rho_{f0} = |\beta_T(T - T_0)| = 1.02 \times 10^{-4} \times (300 - 290) = 1.02 \times 10^{-3}$, which is a very small value.

Fig. 5 shows the particle position and velocity contour or temperature contour at $t = 15$s for simulations with $\rho_r = 1.0068$. The

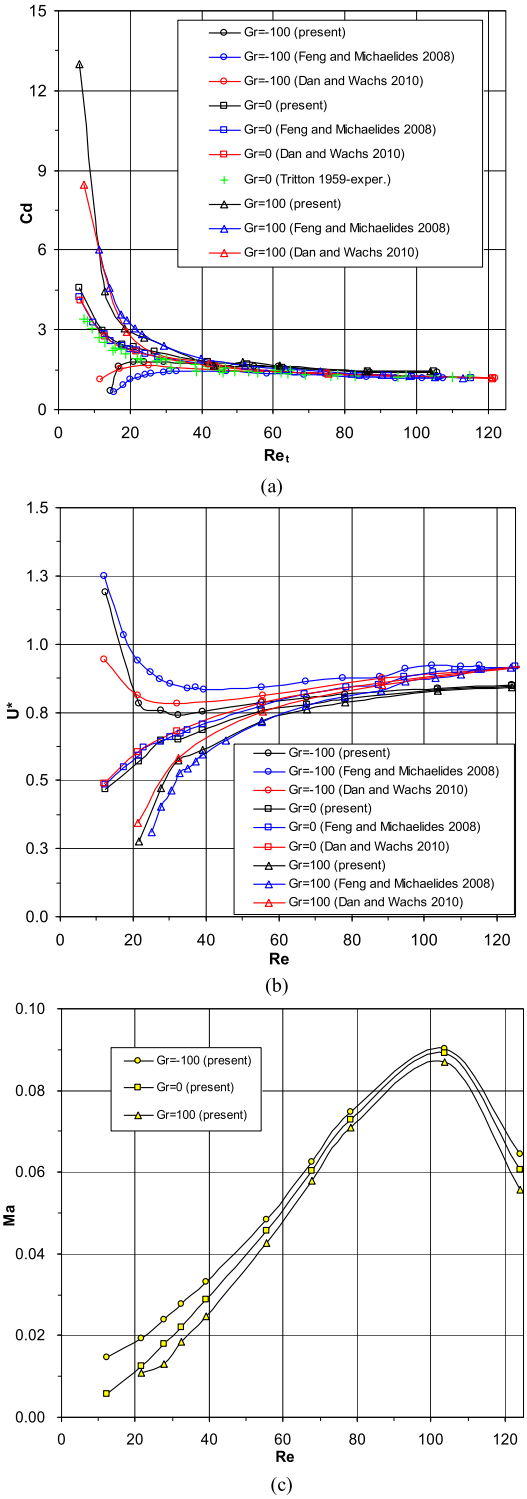

Fig. 4. Variations of the drag coefficient (a), dimensionless terminal velocity (b) and Mach number Ma (c) with the Reynolds number due to different Grashof numbers Gr.

Please cite this article as: Xia M et al., A particle-resolved heat-particle-fluid coupling model by DEM-IMB-LBM, Journal of Rock Mechanics and Geotechnical Engineering, https://doi.org/10.1016/j.jrmge.2023.02.030

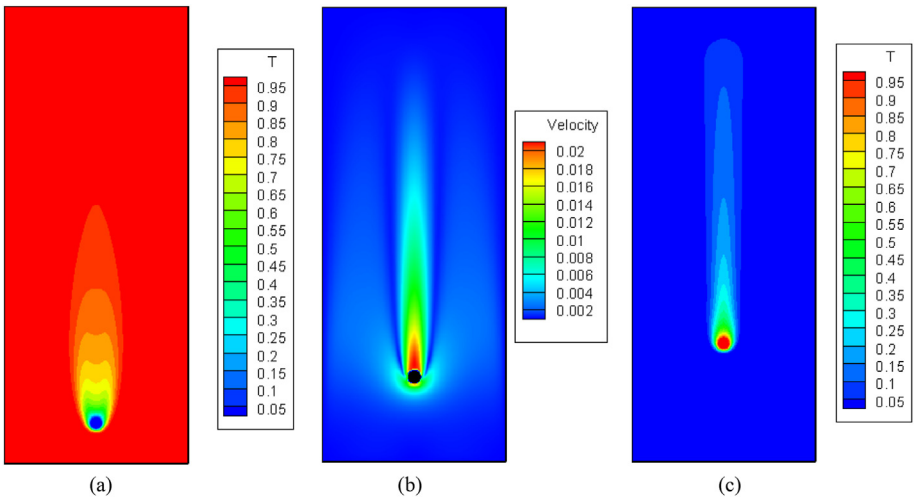

Fig. 5. Particle position at $t = 15$ s ($\rho_r = 1.0068$) (unit: the lattice unit): (a) Temperature contour for a cold particle ($Gr = -100$), (b) Velocity contour for isothermal flow ($Gr = 0$), and (c) Temperature contour for a hot particle ($Gr = 100$).

magnitude of the fluid velocity and temperature are shown in the lattice unit in our simulations, which could be directly converted into physical unit. Within the velocity contour, the maximum fluid velocity with lattice unit is the Mach number. As the Mach number is much smaller than 0.1, the numerical results can be regarded reliable. It is found that the colder particle settles faster than the isothermal and hotter particle cases. Meanwhile, the colder particle has created a wider flume with a shorter tail, while the hot particle has created a narrow flume with a longer tail. These results are also consistent with those of Feng and Michaelides (2008) and Dan and Wachs (2010).

Fig. 6 shows the variations of both vertical position and vertical velocity of the particle under different *Gr* numbers. Compared with the hotter particle or isothermal particle, the colder particle reaches the bottom boundary first. This indicates that the *Gr* number has a considerable effect on the particle motion when the heat transfer between the particle and its surrounding fluid is considered.

3.2. Two-particle DKT simulation with heat transfer

The well-known DKT motion under the isothermal condition has been widely used for validating numerical methods. In this work, this two-particle DKT simulation is revisited with heat transfer between the colder/hotter particle and the fluid as the second benchmark test. As shown in Fig. 7, the computational domain is 0.02 m in width and 0.06 m in height, and divided into 200 × 600 lattice grids with spacing $h = 0.0001$ m. The four boundaries are static walls and thus the no-slip boundary condition is imposed. Meanwhile, all the four boundaries are fully insulated.

Two particles initially located at the positions (0.01 m, 0.052 m) and (0.01 m, 0.048 m) move downward due to gravity. For the fluid, the kinematic viscosity is 1×10^{-6} m^2/s, the density is 1000 kg/m^3, the thermal diffusivity is 1×10^{-6} m^2/s, and the initial temperature is 290 K. For these two particles, the radius is 0.001 m; the density is 1010 kg/m^3; the temperature is 300 K; the friction coefficient and normal stiffness (k_n) are selected as 0.05 and 1×10^7 N/m, respectively; and the tangential stiffness (k_s) is 1×10^7 N/m. The time step for DEM and LBM are respectively 0.1053×10^{-4} s and 2×10^{-4} s, resulting in a subcycling number (N_{sub}) of 19 and a lattice speed (c) of 0.5 m/s. Both relaxation time for density (τ_f) and temperature (τ_g) are selected as 0.56, indicating that the *Pr* number is 1. According to Eq. (30), the two thermal expansion coefficients

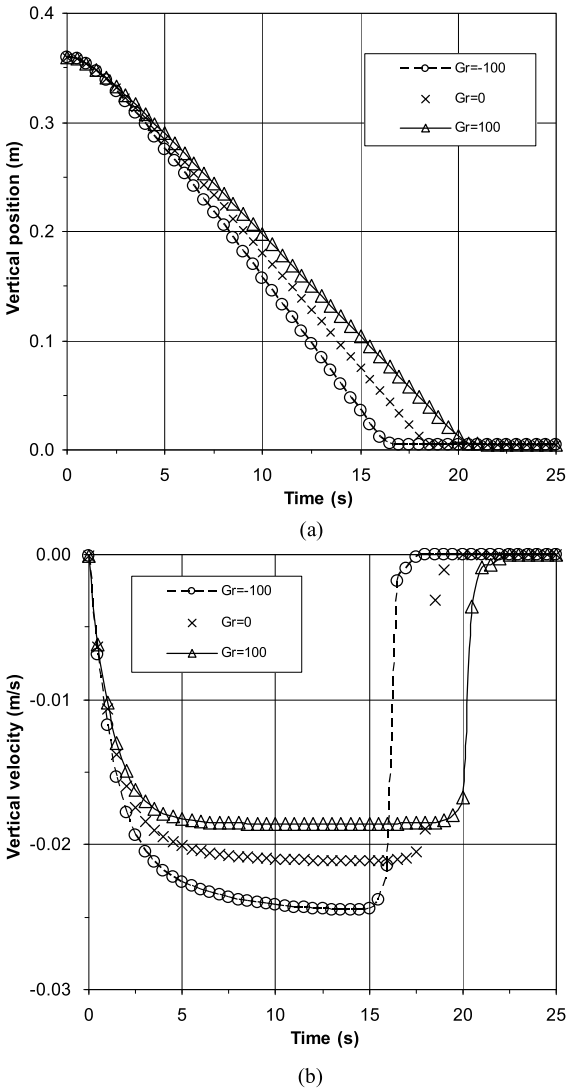

Fig. 6. Variations of the particle vertical position (a) and vertical velocity (b) under different *Gr* numbers ($\rho_r = 1.0068$).

Please cite this article as: Xia M et al., A particle-resolved heat-particle-fluid coupling model by DEM-IMB-LBM, Journal of Rock Mechanics and Geotechnical Engineering, https://doi.org/10.1016/j.jrmge.2023.02.030

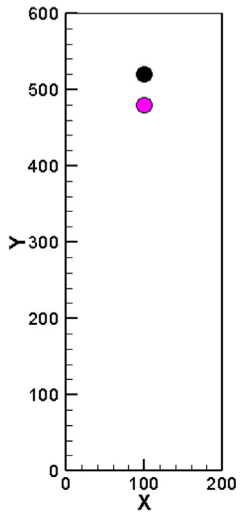

Fig. 7. Two particle sedimentation in an enclosure (unit: the lattice unit).

($\beta_T = 0$ and 1.274×10^{-4} K^{-1}) yield two Gr numbers ($Gr = 0$ and 100). The simulated maximum fluid velocity is $U_{max} = 0.01869$ m/s when $Gr = 0$. Thus, the corresponding Mach number is calculated as $Ma = U_{max}/c = 0.03739$, indicating that the results obtained are reasonably accurate.

To compare our numerical results with those of Feng and Michaelides (2008) and Tao et al. (2021), the following three parameters are calculated:

$$U_{ref} = \sqrt{|g_y| L_{ref}}, L_{ref} = 2R_p, t_{ref} = L_{ref} \Big/ U_{ref} = \sqrt{L_{ref} \Big/ |g_y|} \tag{33}$$

where t_{ref} is the reference time.

Fig. 8 shows the particle positions and fluid velocities or temperature contour at different dimensionless time instants under different Grashof numbers ($Gr = 0$: an isothermal particle, and $Gr = 100$: a hotter particle). As shown in Fig. 8, three stages of the DKT motion can been reproduced when $Gr = 0$ and 100. However, the three stages of the DKT motion are delayed when the heat transfer between the particles and the fluid is accounted for. When $Gr = 0$, two particles finish tumble at $t/t_{ref} = 168$, while they still stay tumble when $Gr = 100$. This result agrees well with Feng and Michaelides (2008) and Tao et al. (2021).

To quantitatively compare with some existing results obtained by the IBM-LBM (Tao et al., 2021) and direct numerical simulations (Feng and Michaelides, 2008), the variations of the dimensionless particle vertical velocity under different Gr numbers are displayed in Fig. 9. A good agreement can be found for both the isothermal

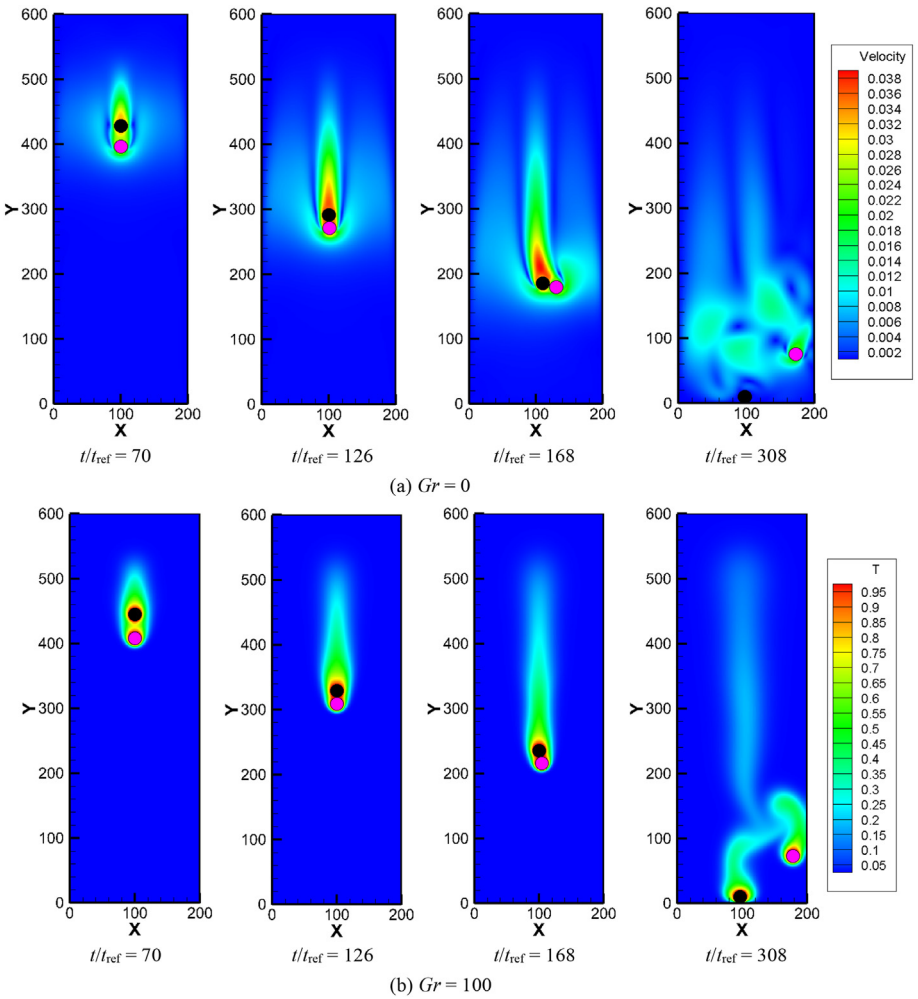

Fig. 8. Particle positions and fluid velocities (a) and temperature contour (b) at different dimensionless time instants under different Grashof numbers Gr (unit: the lattice unit).

Please cite this article as: Xia M et al., A particle-resolved heat-particle-fluid coupling model by DEM-IMB-LBM, Journal of Rock Mechanics and Geotechnical Engineering, https://doi.org/10.1016/j.jrmge.2023.02.030

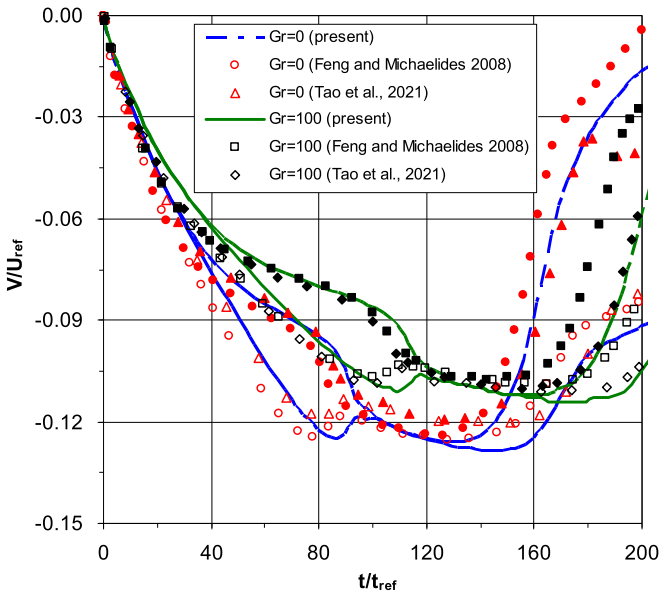

Fig. 9. Variations of the dimensionless particle vertical velocity under different Grashof numbers *Gr* (the filled scatters for the top particle, and the hollow scatters for the bottom particle).

($Gr = 0$) and non-isothermal ($Gr = 100$) cases, demonstrating the accuracy of the proposed model. As shown in Fig. 9, hotter particles fall slowly (i.e. $Gr = 100$) compared to isothermal particles (i.e. $Gr = 0$), which is consistent with the observation of the above single-particle sedimentation simulations with heat transfer in Section 3.1. It also can be seen that the typical DKT phenomenon is clearly observed in both cases. When $Gr = 0$, the drafting stage begins from $t/t_{ref} = 33.6$, the kissing stage starts at $t/t_{ref} = 101$, and the two particles begin to tumble at $t/t_{ref} = 126$. Similarly, when $Gr = 100$, the drafting stage starts at $t/t_{ref} = 44.8$, the kissing stage starts at $t/t_{ref} = 120$, and the two particles begin to tumble at $t/t_{ref} = 162$. It is apparent that the three stages of the DKT motion are

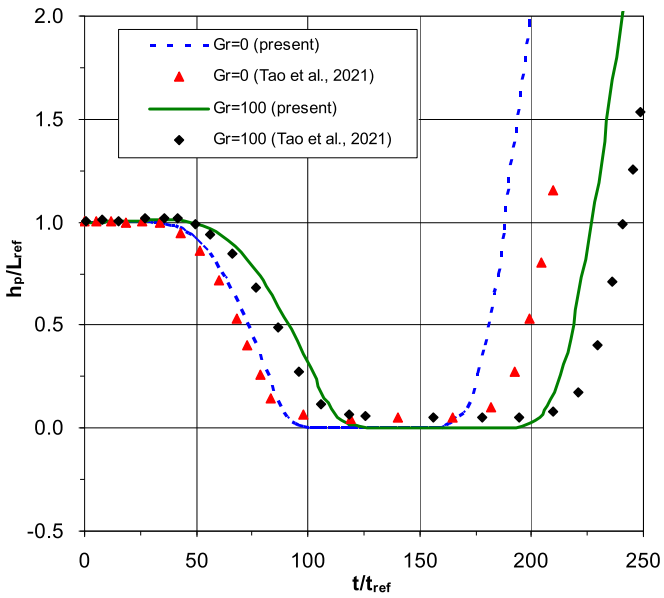

Fig. 10. Variations of the dimensionless gap distance between particles under different Grashof numbers *Gr*.

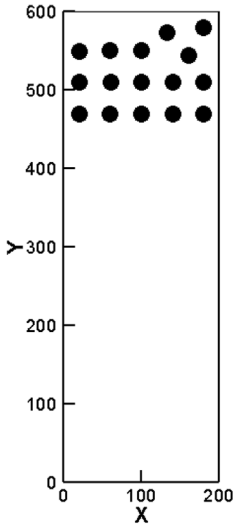

Fig. 11. Sedimentation of 16 particles in an enclosure (unit: the lattice unit).

delayed when the heat transfer between particles and the fluid is accounted for. The reason for this is that the hotter particle will cause the extra buoyancy force which is opposite to the direction of motion.

Meanwhile, from Fig. 9b, the maximum dimensionless particle vertical velocity (V/U_{ref}) is -0.128 when $Gr = 0$. In this situation, the corresponding maximum particle vertical velocity (V_{max}) is 0.01672 m/s. In this extreme case, the accumulated displacement of the particle (l_{max}) during N_{sub} DEM subcycling is $l_{max} = V_{max} N_{sub} \Delta t_{DEM} = 0.01672 \times 19 \times 0.1053 \times 10^{-4} = 0.03344 \times 10^{-4}$ m. Since this value is much lower than the grid cell spacing h (i.e. 0.0001 m), the present value for the sub-cycling number ($N_{sub} = 19$) is still accurate for modeling the present problem.

Fig. 10 depicts the variations of the dimensionless distance between the two particles under different Grashof numbers. As shown in Fig. 10, the three stages of the DKT motion can be seen when $Gr = 0$ or 100. During the sedimentation process, the hotter particles heat up the fluid and cause an extra buoyancy force applied to the particles, resulting in the delay of the DKT process. This numerical result is consistent with Tao et al. (2021) as well. Compared with Tao et al. (2021), the present numerical model can accurately model the kissing state, in which the particle gap distance should be close to 0.

4. Complicated particle-fluid interaction problems with heat transfer

In this section, two multiple-particle simulations with heat transfer (a 16-particle sedimentation problem and a 10-particle migration problem in periodic boundary condition (PBC)) are conducted to further investigate the role of heat transfer in particle-fluid interactions, and to demonstrate the robustness of the coupled thermal DEM-IMB-LBM model proposed in this work. Meanwhile, all particle assembles in this section are generated using the efficient discs packing algorithm developed by Xu and Xia (2023).

4.1. Multiple-particle sedimentation with heat transfer

In this multiple-particle sedimentation simulation case, the time step for DEM and LBM are 0.1064×10^{-4} s and 0.5×10^{-3} s, respectively, leading to the sub-cycling number of DEM in an LBM

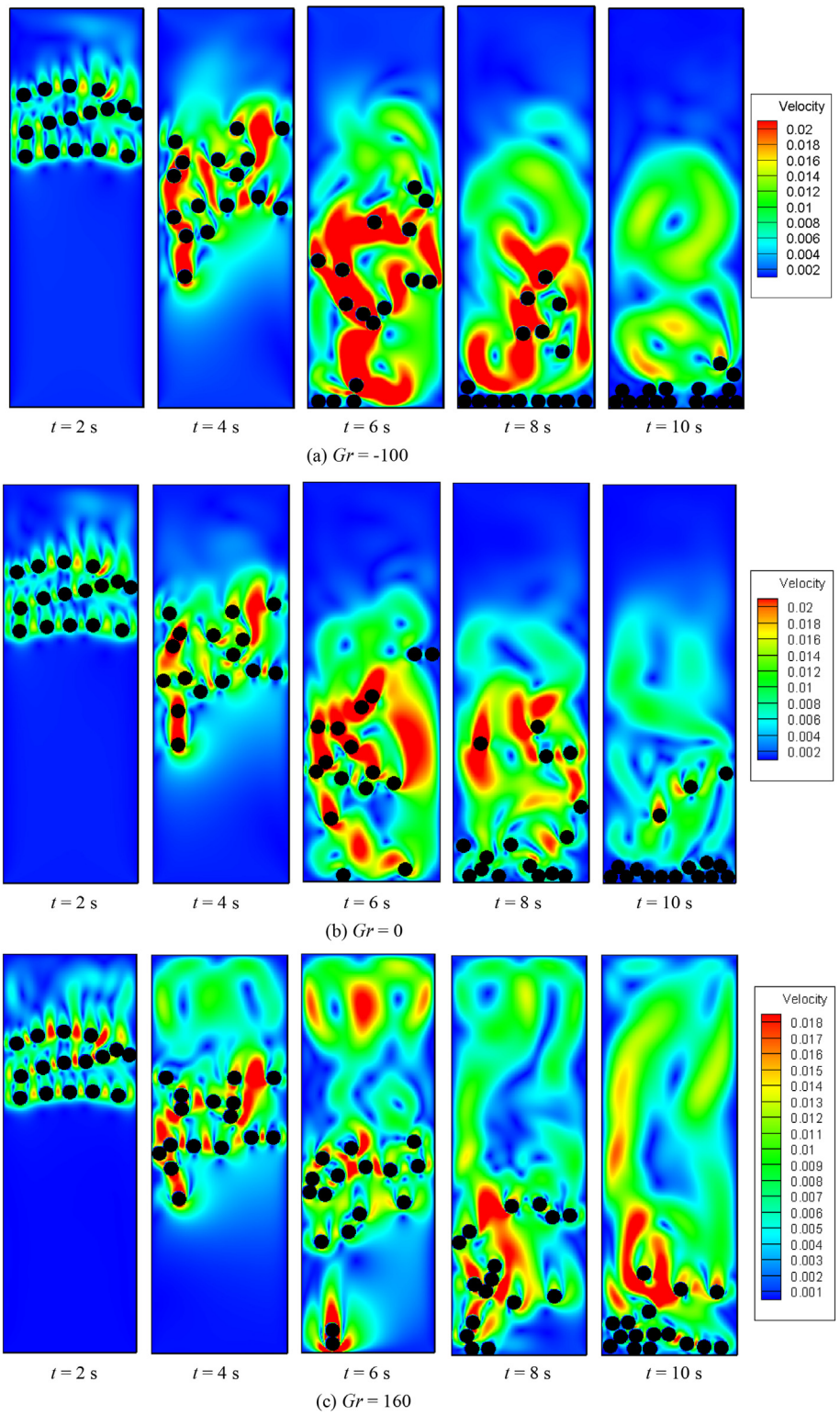

Fig. 12. Evolution of fluid velocity during the settling process at different time instants (unit: the lattice unit).

time step to be 47. Both relaxation time for temperature (τ_g) and fluid density (τ_f) are 0.65, indicating that the *Pr* number is 1. The friction coefficient between the particles is 0.05. Other parameters of the particles and the fluid used in this section are the same with those in the two-particle DKT simulation in Section 3.2. In this numerical example, 16 particles with the same radius are considered as shown in Fig. 11. Three different Grashof numbers are also considered in the simulation: $Gr = -100$, 0 and 160. The simulated maximum fluid velocity is $U_{max} = 0.02289$ m/s when $Gr = -100$. Thus, the corresponding Mach number is calculated as $Ma = U_{max}/c = 0.04578$, indicating that the results obtained are reasonably accurate.

Please cite this article as: Xia M et al., A particle-resolved heat-particle-fluid coupling model by DEM-IMB-LBM, Journal of Rock Mechanics and Geotechnical Engineering, https://doi.org/10.1016/j.jrmge.2023.02.030

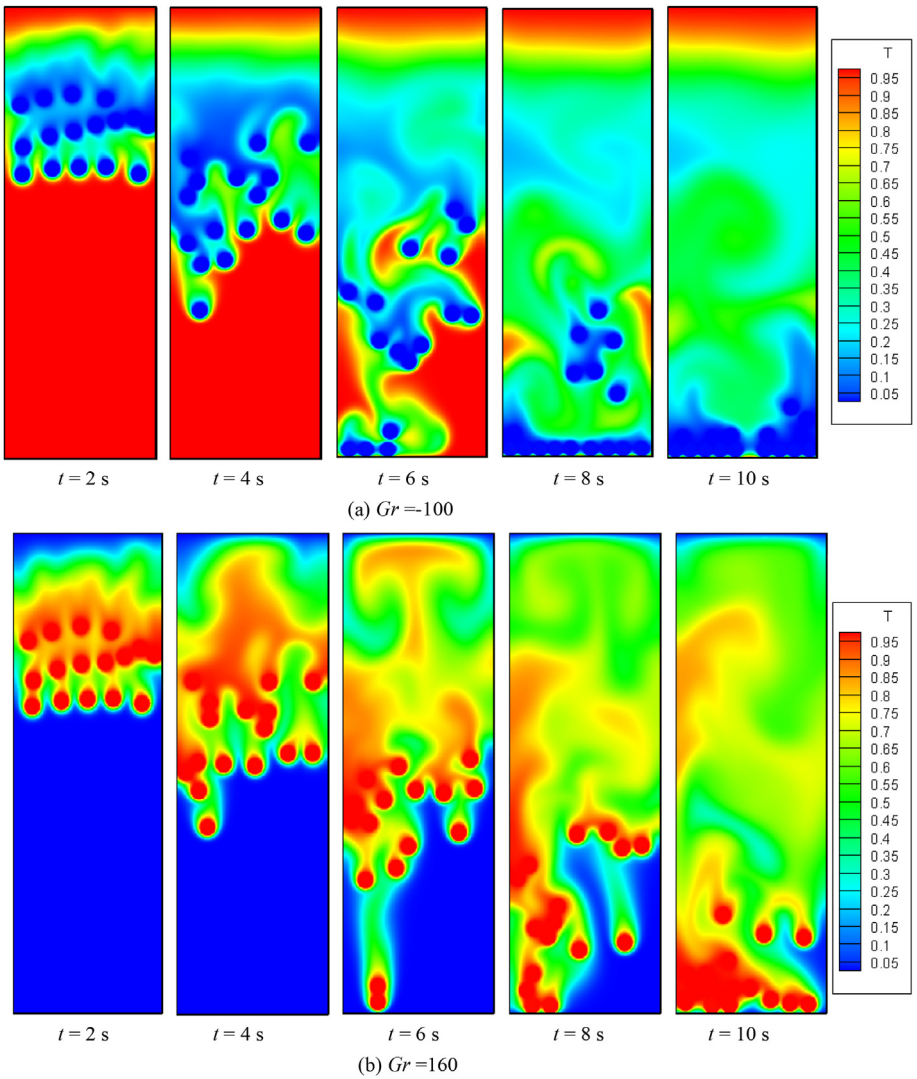

Fig. 13. Evolution of temperature contours during the settling process at different time instants.

Fig. 12 shows the evolution of fluid velocity during the settling process for $Gr = -100$, 0 and 160 at different time instants. From the fluid velocity contours in Fig. 12, we can see that the positions of the particles have a minor difference under different Gr numbers at the early stage of sedimentation ($t = 2$ s). However, most particles reach the bottom of the enclosure at the time $t = 8$ s when $Gr = -100$, while only two particles reach the bottom of the enclosure when $Gr = 160$. Furthermore, the final particle distribution is totally different under different Gr numbers, which indicates that the heat transfer between the particle and the fluid has a significant effect on particle-laden flows. Fig. 13 displays the evolution of temperature contours during the settling process at different time instants. It is found that the movement of hotter particles is slower, and apparent heat transfer from the hotter particle to the fluid can be observed. For this reason, the fluid temperature at the top of the enclosure is heated up. However, as the colder particles move downward in Fig. 13a, the fluid temperature at the top of the enclosure is not cooled down at the end of the simulation ($t = 10$ s).

In the previous simulations, the temperatures of all particles are the same. To further demonstrate that the proposed method solves the problems with non-uniform particle temperatures, the temperatures of 16 particles are set in the range of 290–300 K. Other parameters of the particles and the fluid are the same as those in the $Gr = 160$ simulation in this section. Fig. 14 shows the evolution of fluid velocity and temperature contours during the settling process for different particle temperatures at different time instants. It can be seen that the particle temperature has a considerable effect on particle laden motion. Meanwhile, when the heat is transferred from the particles to the surrounding fluid, the temperature field is totally different.

4.2. Multiple-particle migration with heat transfer in a Poiseuille flow

In this part, a multiple-particle migration with heat transfer in a Poiseuille flow is carried out. When a fluid-particle system contains a larger number of particles, it is necessary to parallelize the DEM-

Please cite this article as: Xia M et al., A particle-resolved heat-particle-fluid coupling model by DEM-IMB-LBM, Journal of Rock Mechanics and Geotechnical Engineering, https://doi.org/10.1016/j.jrmge.2023.02.030

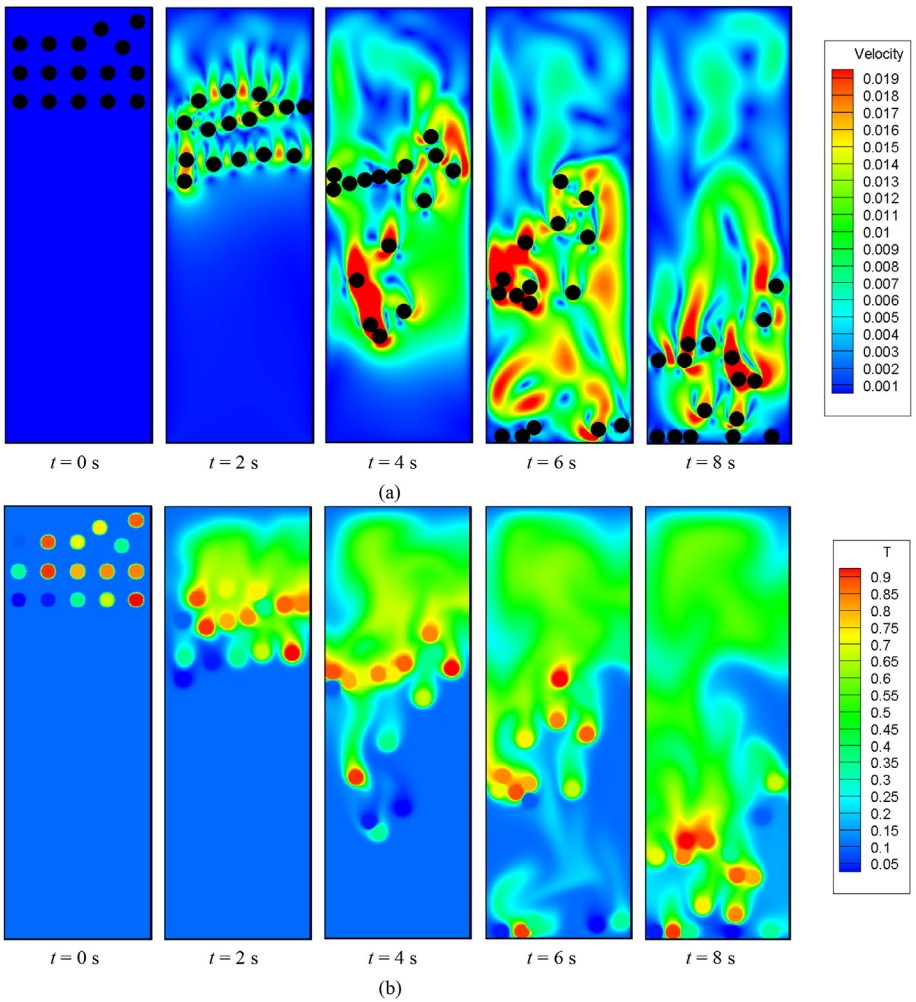

Fig. 14. Evolution of fluid velocity (a) and temperature contours (b) during the settling process with different particle temperatures at different time instants (unit: the lattice unit).

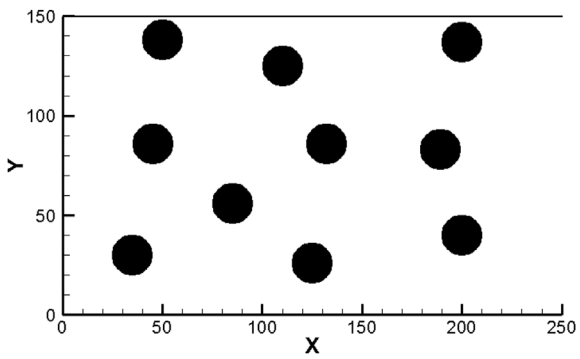

Fig. 15. Migration of 10 particles in an infinite tube (unit: the lattice unit).

LBM approach to reduce the computational cost. An alternative way is to employ the PBC in the DEM-LBM framework. The PBC can be used for approximating a large (infinite) system by using a small part called a unit cell with fewer particles (Wang et al., 2017b). Obviously, the computation cost of using PBC can be greatly reduced by reducing the number of particles required. The PBC was firstly implemented by Wang et al. (2017b) into the DEM-IMB-LBM framework for modeling fluid-solid interaction problems. This PBC for DEM-IMB-LBM mainly contains three parts: the interaction and periodic migration of solid particles, the fluid-solid coupling at the periodic boundary and the periodic flow of fluid. When heat transfer between particles and fluids is considered in a periodic computational domain, the PBC for heat transfer needs to be applied. Recently, an efficient and robust PBC algorithm proposed by Xia et al. (2023) to model mass transport and particle dissolution problems is used in the present study. The detail algorithm can be found in Xia et al. (2023).

A total of 10 circular particles with the same radius of 0.001 m are randomly positioned in a Poiseuille flow. As shown in Fig. 15, the computational domain is 0.025 m $\times$ 0.015 m, and divided into 250 $\times$ 150 lattice grids with spacing $h = 0.0001$ m. For the fluid, the kinematic viscosity is 1×10^{-4} m^2/s, the density is 1000 kg/m^3, the thermal diffusivity is 1×10^{-4} m^2/s, and the initial temperature is 290 K. For these particles, the density is 1000 kg/m^3, the temperature is 300 K, and the normal stiffness (k_n) is 1×10^6 N/m. The friction between these particles is ignored. The relaxation time for density (τ_f) and temperature (τ_g) is 0.8, indicating that the Pr number is 1. The densities of the particles and the fluid are both equal to 1000 kg/m^3, indicating that all particles are in a neutrally buoyant condition. The no-slip boundaries are imposed at the top and bottom boundaries for the fluid field, while these two boundaries are fully insulated. A constant pressure boundary condition with $\rho_{in} = 1003$ kg/m^3 and $\rho_{out} = 1000$ kg/m^3 are imposed to

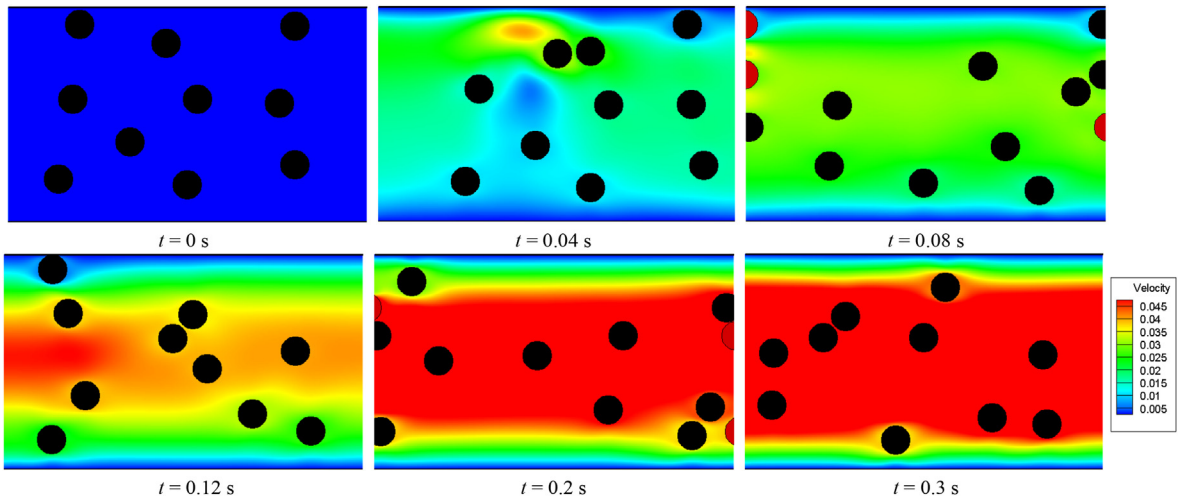

Fig. 16. Evolution of fluid velocity and particle positions during the migration process at different time instants (unit: the lattice unit).

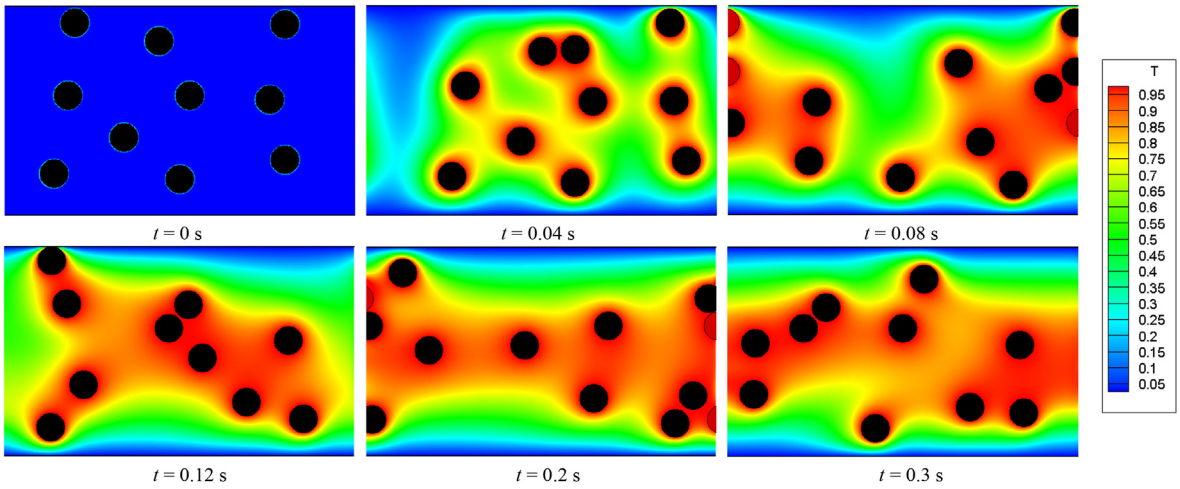

Fig. 17. Evolution of temperature contours during the migration process at different time instants (unit: the lattice unit).

the left inlet and right outlet, respectively, indicating that fluid and particles will move along the horizontal direction under the pressure-driven force.

In the PBC, when a particle exceeds the right boundary, it will re-enter the computation domain from the left boundary. At the same time, when the particle and fluid with a certain temperature leave the domain on the right boundary, it will re-enter at the left boundary with the same temperature. Initially, the temperature of the fluid (T_0) is 290 K, and the initial velocities of the fluid and all particles are zero. During the whole simulation process, all the particle temperatures are fixed to 291 K. Meanwhile, the thermal expansion coefficient ($\beta_T = 0\ \mathrm{K}^{-1}$) is considered, meaning that the fluid density is not changed due to the temperature effect. Both the LBM and DEM time steps are 1×10^{-5} s, resulting in the sub-cycling number of DEM within one LBM step to be 1. The simulated maximum fluid velocity is $U_{\max} = 0.04124$ m/s. Thus, the corresponding Mach number is calculated as $Ma = U_{\max}/c = 0.08247$, indicating that the results obtained are reasonably accurate.

Fig. 16 displays the evolution of fluid velocity and particle positions during the migration process at different time instants, while Fig. 17 displays the evolution of temperature contours during the migration process at different time instants. It can be seen that fluid and particles start to move from the left to right when a larger pressure is applied at the left boundary. At $t = 0.04$ s, the temperature of fluid around particle has been increased due to heat transfer from hotter particles. At $t = 0.08$ s, some particles (marked in red) move out of the right boundary and re-enter the domain from the left inlet. Most particles are concentrated in the middle part of the domain in the Poiseuille flow. Thus, hot area is concentrated on the middle part of the domain ($t = 0.3$ s). The migration process of particles is successfully simulated, which demonstrates the robustness of the coupled thermal DEM-IMB-LBM model as well.

5. Conclusions

This paper enhances a particle-resolved heat-particle-fluid coupling model (DEM-IMB-LBM) to solve heat-particle-fluid coupling problems. The main conclusions can be summarized as follows.

(1) The thermal LBM is incorporated into the conventional DEM-LBM to simulate heat transfer, and the IMB is extended to

Please cite this article as: Xia M et al., A particle-resolved heat-particle-fluid coupling model by DEM-IMB-LBM, Journal of Rock Mechanics and Geotechnical Engineering, https://doi.org/10.1016/j.jrmge.2023.02.030

achieve Dirichlet-type temperature boundary conditions at the interface between the moving particles and the fluid.

(2) Four numerical examples (single-particle sedimentation, two-particle DKT simulation, multiple-particle sedimentation with heat transfer, and multiple-particle migration in a computational domain with heat transfer) have demonstrated the accuracy and capability of the proposed coupling technique.

(3) Heat transfer between particles and fluid flows has a considerable effect on particle motion in complex disperse multiphase flows.

Since the inter-particle collision process is instantaneous and the contact duration time among particles is very small in a dilute particle system, it is reasonable to ignore heat conduction among solid particles. However, for dense particle-laden flows, heat conduction between solid particles cannot be neglected. Then, the heat conduction model (i.e. DTEM) proposed by Feng et al. (2008, 2009) between solid particles in contact can be used. Recently, the DTEM has been implemented into the disk discontinuous deformation analysis method to simulate heating particles (Huang et al., 2022). These extensions will be reported later for the simulations of dense fluid-particle systems.

Declaration of competing interest

The authors declare that they have no known competing financial interests or personal relationships that could have appeared to influence the work reported in this paper.

Acknowledgments

This work is financially supported by the Natural Science Foundation of Hunan Province, China (Grant No. 2022JJ30567), the support of EPSRC Grant (UK): PURIFY (EP/V000756/1), and the Scientific Research Foundation of Education Department of Hunan Province, China (Grant No. 20B557).

References

Chen, S., Doolen, G., 1998. Lattice Boltzmann method for fluid flows. Annu. Rev. Fluid Mech. 30, 329–364.
Chen, Y., Müller, C.R., 2020. A Dirichlet boundary condition for the thermal lattice Boltzmann method. Int. J. Multiphas. Flow 123, 103184.
Chun, B., Ladd, A.J.C., 2007. Interpolated boundary condition for lattice Boltzmann simulations of flows in narrow gaps. Phys. Rev. E 75 (6), 066705.
Cook, B.K., Noble, D.R., Williams, J.R., 2004. A direct simulation method for particle-fluid systems. Eng. Comput. 21 (2–3), 151–168.
Cundall, P.A., Strack, O.D.L., 1979. A discrete numerical model for granular assemblies. Geotechnique 29 (1), 47–65.
Dan, C., Wachs, A., 2010. Direct Numerical Simulation of particulate flow with heat transfer. Int. J. Heat Fluid Flow 31 (6), 1050–1057.
Feng, Y.T., Han, K., Owen, D.R.J., 2007. Coupled lattice Boltzmann method and discrete element modelling of particle transport in turbulent fluid flows: computational issues. Int. J. Numer. Methods Eng. 72 (9), 1111–1134.
Feng, Y.T., Han, K., Li, C.F., Owen, D.R.J., 2008. Discrete thermal element modelling of heat conduction in particle systems: basic formulations. J. Comput. Phys. 227 (10), 5072–5089.
Feng, Y.T., Han, K., Owen, D.R.J., 2009. Discrete thermal element modelling of heat conduction in particle systems: pipe-network model and transient analysis. Powder Technol. 193 (3), 248–256.
Feng, Y.T., Han, K., Owen, D.R.J., 2010. Combined three-dimensional lattice Boltzmann method and discrete element method for modelling fluid-particle interactions with experimental assessment. Int. J. Numer. Methods Eng. 81, 229–245.
Feng, Y.T., 2021a. An energy-conserving contact theory for discrete element modelling of arbitrarily shaped particles: basic framework and general contact model. Comput. Methods Appl. Mech. Eng. 373, 113454.
Feng, Y.T., 2021b. An energy-conserving contact theory for discrete element modelling of arbitrarily shaped particles: contact volume based model and computational issues. Comput. Methods Appl. Mech. Eng. 373, 113493.
Feng, Y.T., 2023. Thirty years of developments in contact modelling of non-spherical particles in DEM: a selective review. Acta Mech. Sin. 39, 722343.
Feng, Z.-G., Michaelides, E.E., 2008. Inclusion of heat transfer computations for particle laden flows. Phys. Fluids 20, 675–684.
Fu, J.L., Dong, J.B., Wang, Y.L., Ju, Y., Owen, D.R.J., Li, C.F., 2020. Resolution effect: an error correction model for intrinsic permeability of porous media estimated from lattice Boltzmann method. Transport Porous Media 132 (3), 627–656.
Galindo-Torres, S., 2013. A coupled discrete element lattice Boltzmann method for the simulation of fluid–solid interaction with particles of general shapes. Comput. Methods Appl. Mech. Eng. 265, 107–119.
Guo, Z., Zheng, C., Shi, B., 2002. Discrete lattice effects on the forcing term in the lattice Boltzmann method. Phys. Rev. E 65, 046308.
Han, Y., Cundall, P.A., 2013. LBM-DEM modeling of fluid-solid interaction in porous media. Int. J. Numer. Anal. Methods GeoMech. 37 (10), 1391–1407.
Honari, S., Seyedi Hosseininia, E., 2021. Particulate modeling of sand production using coupled DEM-LBM. Energies 14, 906.
Hu, J., Guo, Z., 2017. A numerical study on the migration of a neutrally buoyant particle in a Poiseuille flow with thermal convection. Int. J. Heat Mass Tran. 108, 2158–2168.
Hu, Y., Li, D., Shu, S., Niu, X., 2016. An efficient immersed boundary-lattice Boltzmann method for the simulation of thermal flow problems. Commun. Comput. Phys. 20 (5), 1210–1257.
Huang, G.H., Tong, C.X., Zhang, S., Chen, X.F., 2022. A thermo-solid coupling model for disk discontinuous deformation analysis to simulate heating and stirring particles in rotary drums. Powder Technol. 402, 117326.
Kang, S.K., Hassan, Y.A., 2011. A direct-forcing immersed boundary method for the thermal lattice Boltzmann method. Comput. Fluids 49 (1), 36–45.
Kang, Q.J., Lichtner, P.C., Zhang, D.X., 2007. An improved lattice Boltzmann model for multicomponent reactive transport in porous media at the pore scale. Water Resour. Res. 43 (12), W12S14.
Ladd, A.J.C., 1994. Numerical simulations of particulate suspensions via a discretized Boltzmann equation: Part 1. Theoretical foundation. J. Fluid Mech. 271, 285–309.
Liu, W., Wu, C.Y., 2019. Analysis of inertial migration of neutrally buoyant particle suspensions in a planar Poiseuille flow with a coupled lattice Boltzmann method-discrete element method. Phys. Fluids 31 (6), 063301.
McCullough, J.W.S., Aminossadati, S.M., Leonardi, C.R., 2020. Transport of particles suspended within a temperature-dependent viscosity fluid using coupled LBM–DEM. Int. J. Heat Mass Tran. 149, 119159.
McCullough, J.W.S., Łaniewski-Wołłk, Ł., Aminossadati, S.M., Leonardi, C.R., 2021. A 3D LBM-DEM study of sheared particle suspensions under the influence of temperature-dependent viscosity. Powder Technol. 390, 143–158.
Noble, D.R., Torczynski, J.R., 1998. A lattice-Boltzmann method for partially saturated computational cells. Int. J. Mod. Phys. C 9 (8), 1189–1201.
O'Sullivan, C., 2011. Particulate Discrete Element Modelling: A Geomechanics Perspective. CRC Press, London.
Owen, D.R.J., Leonardi, C.R., Feng, Y.T., 2011. An efficient framework for fluid–structure interaction using the lattice Boltzmann method and immersed moving boundaries. Int. J. Numer. Methods Eng. 87, 66–95.
Peskin, C.S., 1977. Numerical analysis of blood flow in the heart. J. Comput. Phys. 25 (3), 220–252.
Qian, Y.H., D'Humieres, D., Lallemand, P., 1992. Lattice BGK models for Navier–Stokes equation. Europhys. Lett. 17 (6), 479–484.
Qu, T., Wang, M., Feng, Y., 2022. Applicability of discrete element method with spherical and clumped particles for constitutive study of granular materials. J. Rock Mech. Geotech. Eng. 14 (1), 240–251.
Rosemann, T., Kravets, B., Reinecke, S.R., Kruggel-Emden, H., Wu, M., Peters, B., 2019. Comparison of numerical schemes for 3D lattice Boltzmann simulations of moving rigid particles in thermal fluid flows. Powder Technol. 356, 528–546.
Suzuki, K., Kawasaki, T., Furumachi, N., Tai, Y., Yoshino, M., 2018. A thermal immersed boundary–lattice Boltzmann method for moving-boundary flows with Dirichlet and Neumann conditions. Int. J. Heat Mass Tran. 121, 1099–1117.
Tao, S., He, Q., Chen, B., Qin, G.F., 2021. Distribution function correction-based immersed boundary lattice Boltzmann method for thermal particle flows. Comput. Part. Mech. 8, 459–469.
Tritton, J.D., 1959. Experiments on the flow past a circular cylinder at low Reynolds numbers. J. Fluid Mech. 6 (4), 547–567.
Wang, D., Leonardi, C.R., Aminossadati, S.M., 2018. Improved coupling of time integration and hydrodynamic interaction in particle suspensions using the lattice Boltzmann and discrete element methods. Comput. Math. Appl. 75 (7), 2593–2606.
Wang, D., You, Z., Wang, M., Li, Q., Wu, L., 2022a. Numerical investigation of proppant transport at hydraulic-natural fracture intersection. Powder Technol. 398, 117123.
Wang, D., Li, S., Zhang, D., Pan, Z., 2023. Understanding and predicting proppant bedload transport in hydraulic fracture via numerical simulation. Powder Technol. 417, 118232.

Please cite this article as: Xia M et al., A particle-resolved heat-particle-fluid coupling model by DEM-IMB-LBM, Journal of Rock Mechanics and Geotechnical Engineering, https://doi.org/10.1016/j.jrmge.2023.02.030

Wang, M., Feng, Y.T., Wang, Y., Zhao, T.T., 2017b. Periodic boundary conditions of discrete element method-lattice Boltzmann method for fluid-particle coupling. Granul. Matter 19 (3), 43.
Wang, M., Feng, Y.T., Pande, G.N., Chan, A.H.C., Zuo, W.X., 2017a. Numerical modelling of fluid-induced soil erosion in granular filters using a coupled bonded particle lattice Boltzmann method. Comput. Geotech. 82, 134–143.
Wang, M., Feng, Y.T., Owen, D.R.J., Qu, T., 2019. A novel algorithm of immersed moving boundary scheme for fluid–particle interactions in DEM-LBM. Comput. Methods Appl. Mech. Eng. 346, 109–125.
Wang, M., Feng, Y.T., Qu, T., Tao, S., Zhao, T., 2020. Instability and treatments of the coupled discrete element and lattice Boltzmann method by the immersed moving boundary scheme. Int. J. Numer. Methods Eng. 121 (21), 4901–4919.
Wang, M., Feng, Y.T., Qu, T.M., Zhao, T.T., 2021. A coupled polygonal DEM-LBM technique based on an immersed boundary method and energy-conserving contact algorithm. Powder Technol. 381, 101–109.
Wang, T., Zhang, F., Furtney, J., Damjanac, B., 2022b. A review of methods, applications and limitations for incorporating fluid flow in the discrete element method. J. Rock Mech. Geotech. Eng. 14 (3), 1005–1024.
Xia, M., 2016. Pore-scale simulation of miscible displacement in porous media using the lattice Boltzmann method. Comput. Geosci. 88, 30–40.
Xia, M., Gong, F.Q., Feng, S., Yu, J., Feng, Y.T., Wang, M., 2023. A coupled DEM-IMB-LBM model for simulating methane hydrate exploitation involving particle dissolution. Int. J. Numer. Methods Eng. 124 (8), 1701–1720.
Xu, X., Xia, M., 2023. An efficient algorithm for dense discs packing considering domain boundaries. J. Xiangtan Univ. Nat. Sci. Ed. 45 (2), 18–28.
Zhang, H., Yu, A., Zhong, W., Tan, Y., 2015. A combined TLBM–IBM–DEM scheme for simulating isothermal particulate flow in fluid. Int. J. Heat Mass Tran. 91, 178–189.
Zhang, P., Galindo-Torres, S.A., Tang, H., Jin, G., Scheuermann, A., Li, L., 2016. Lattice Boltzmann simulations of settling behaviors of irregularly shaped particles. Phys. Rev. E 93 (6), 062612.
Zhang, P., Galindo-Torres, S.A., Tang, H., Jin, G., Scheuermann, A., Li, L., 2017. An efficient Discrete Element Lattice Boltzmann model for simulation of particle-fluid, particle-particle interactions. Comput. Fluids 147, 63–71.

Dr. Ming Xia is an Associate Professor in the College of Civil Engineering at Xiangtan University, China. He obtained his BSc, MSc and PhD degrees from Central South University, China, in 2007, 2009 and 2014, respectively. During November 2019 to November 2020, he conducted research work on the combined DEM and LBM under supervision of Professor Y.T. Feng at the Zienkiewicz Centre for Computational Engineering, Swansea University (UK). His research interests include: (1) multifield/multiphysics coupling of rock mechanics and its application, and (2) computational methods in porous media. He presided 2 projects funded by the National Natural Science Foundation of China and 4 projects funded by the Hunan Province.

Dr. Jinlong Fu is a postdoctoral researcher at the Zienkiewicz Institute for Modelling, Data and AI at Swansea University. He obtained his PhD in computational mechanics from Swansea University in 2020, and he won the Best PhD Thesis Award in the UK Association for Computational Mechanics (the Roger Owen Prize, 2021). He has a multidisciplinary research background with research experience at the interface of computational mechanics, numerical simulation, data science, physics-based engineering modeling, and AI. His broad research interests focus on pore-scale flow modeling, computational fluid dynamics, model order reduction and high-performance computing. The goal of his research is to model and simulate physical systems at different scales by integrating simulation, modeling and AI; and to provide strategies for system learning, prediction, optimization and decision-making in real time.

Please cite this article as: Xia M et al., A particle-resolved heat-particle-fluid coupling model by DEM-IMB-LBM, Journal of Rock Mechanics and Geotechnical Engineering, https://doi.org/10.1016/j.jrmge.2023.02.030